# Optical, electrical and morphological study of PEDOT:PSS single layers spiral-bar coated with various secondary doping solvents.

Tomas Syrovy[1,2], Petr Janicek[*,3,2], Jan Mistrik[3,2], Karel Palka[4,2], Petra Hawlova[1], Lubomir Kubac[5] and Marta Klanjšek Gunde[6]

[1] Department of Graphic Arts and Photophysics, Faculty of Chemical Technology, University of Pardubice, Technological Pavilion Doubravice 41, 53353 Pardubice, Czech Republic

[2] Center of Materials and Nanotechnologies, Faculty of Chemical Technology, University of Pardubice, Studentska 95, 53210 Pardubice, Czech Republic

[3] Institute of Applied Physics and Mathematics, Faculty of Chemical Technology, University of Pardubice, Studentska 95, 53210 Pardubice, Czech Republic

[4] Department of General and Inorganic Chemistry, Faculty of Chemical Technology, University of Pardubice, Studentska 95, 53210 Pardubice, Czech Republic

[5] Center for Organic Chemistry s.r.o., Rybitvi 296, 53354 Rybitvi, Czech Republic

[6] National Institute of Chemistry, Hajdrihova 19, SI-1000 Ljubljana, Slovenia

* Corresponding author: e-mail petr.janicek@upce.cz, Phone: +00 420 466 036 442

**Keywords**: PEDOT:PSS, secondary dopants, spiral-bar coating, spectroscopic ellipsometry, electrical properties, morphological properties.

**Abstract:**

The electrical, morphological and optical properties of a series of spiral-bar coated single layers of PEDOT:PSS influenced by the addition of 10 different secondary dopants have been studied. The optical properties of these samples have been analyzed over a broad spectral range from 190 nm to 30 μm using spectroscopic ellipsometry and transmittance. The isotropic model fits the ellipsometric data quite well. No substantial differences in the optical constants were obtained, despite a difference being expected from the significant change of specific electrical conductivity (by 3 orders of magnitude). In the infrared part of spectra, the multiple Lorentz oscillators' model was used instead of the frequently used Drude model by applying narrow oscillators for molecular vibrations together with the broad oscillators describing electronic transitions in the mid-gap states. The geometrical parameters obtained from ellipsometry evaluation have been found to be in good agreement with standard mechanical characterization probes (profilometry and AFM). The highest value of the specific electric conductivity, 78.3 S/cm, was achieved by using n-methyl methanamide as a secondary dopant. The research results confirm that spectroscopic ellipsometry is a valuable tool for characterization of the functional layers used in printed electronics.

## 1 Introduction

Poly(3,4-ethylenedioxythiophene):poly(styrenesulfonate) (PEDOT:PSS) is one of the most promising conducting polymers for industrial applications, such as light emitting diodes, light emitting capacitor,

photovoltaic cells and sensors, organic transistors, and batteries. [1-5] High application importance is given by its high electrical conductivity, reasonable optical transparency in the visible spectral region and good environmental stability. Due to these properties, PEDOT:PSS has become one of the most important and widely used transparent electrode layers or electrically active layers in polymer based, organic electronic devices.

Films of PEDOT:PSS can be easily processed from aqueous dispersions with the presence of different solvents / secondary dopants by various coating or printing techniques. In the literature, other deposition methods (such as an electrospray deposition [6]) are discussed. The physical properties of such layers depend on their morphology, where isotropic and anisotropic behaviour could be present.

It is well known that the addition of solvents, such as ethane-1,2-diol, glycerol, metyl sulfoxide, dimethyl sulfoxide, N,N-dimethylformamide, tetrahydrofuran, N-methylpyrrolidone, 2-nitroethanol, 1-methyl-2-pyrrolidinone, isopropanol, meso-erythritol (1,2,3,4-tetrahydroxybutane) and sorbitol increase the conductivity of PEDOT:PSS by up to 2 or 3 orders of magnitude [7-17].

In the literature PEDOT:PSS films secondary doped with ethylene glycol with the additional solvent post-treatment show enhanced conductivities up to 1418 S/cm attributed to the removal of PSS from PEDOT:PSS layers [7]. For addition of dimethyl sulfoxide increase of conductivity up to 966 S/cm has been reported explained by possible chain extension [8]. Ouyang at al. reported increase of specific conductivity up to 200 S/cm using ethylene glycol, or 143 S/cm using dimethyl sulfoxide, attributed to the increased interchain interaction [9]. For ethylene glycol as secondary dopant conductivity 160 S/cm has been reported by Ouyang at al. attributed to conformational changes [10]. Kim et al. reported specific conductivity 4 S/cm using tetrahydrofuran, 30 S/cm using dimethyl formamide and 80 S/cm using dimethyl sulfoxide explained by screening effect of secondary solvent [11]. Increase of conductivity up to 48 S/cm attributed to morphological changes caused by different secondary solvents and post-treatment was reported by Jönsson et al. [12]. Increase of specific conductivity of PEDOT using methanol as a secondary solvent up to 20 S/cm explained by structural changes has been reported by Kim et al. [13]. Crispin at el. reported enhanced conductivity of PEDOT:PSS up to 10 S/cm using diethylene glycol explained with phase separation of PEDOT and PSS [14]. Improved electric conductivity persists even upon complete removal of solvents from layers with drying.

Other observed effects of secondary dopants on PEDOT:PSS films besides significant improvement of conductivity are saturation of conductivity at a certain concentration, and increased roughness. Several properties are required for suitability of the secondary dopants for PEDOT:PSS, such as high solubility in water, high boiling point and high static dielectric constant.

The transport properties (especially DC electric conductivity) of PEDOT:PSS films prepared by spin coating were found to be strongly anisotropic. In studies [18-19], a quantitative explanation of this behavior was introduced in terms of the morphological model in which flattened, quasimetallic PEDOT-rich grains are organized in horizontal layers, separated by continuous insulating PSS lamellas (“lasagna-like structure”). It is believed that charge transport in PEDOT:PSS occurs via a hopping process.

Another morphological model uses the idea of transformation of the shape of PEDOT-rich grains from short-curved domains to a long-stretched network (conformation change) that lead to larger grain sizes and lower inter-grain hopping barriers by solvent post treatment [7, 10]. The driving force for this effect was shown to be the interaction between the dipoles of the secondary dopant and dipoles or charges on the PEDOT chains or depletion of insulating PSS, which results in the development of a compact thin film structure with PEDOT-rich

granular networks. Such a network generates larger contact areas between better oriented PEDOT-rich grains, resulting in the improved conductivity due to enhanced conducting pathways for carriers. An increase in the apparent size of the PEDOT-rich particles was reported by Timpanaro et al. [21].

Assuming isotropic optical properties of PEDOT:PSS layers, the pseudo-dielectric constant was measured by in-situ ellipsometry to study their growth onto flexible polymeric substrates [22]. Isotropic optical behavior was also reported in the case of PEDOT:PSS prepared by the electrospray method [6]. Anisotropic optical properties were reported by Petterson et al. [23-24] for spin coated PEDOT and PEDOT:PSS thin layers. The optical properties were studied by variable angle spectroscopic ellipsometry in combination with reflection and transmission measurements.

The uniaxial anisotropy of PEDOT films reveals different ordinary (in-plane showing metallic character) and extraordinary (out-of-plane) indices of refraction. Petterson et al. [24] studied PEDOT:PSS layers prepared from dispersions with sorbitol. A higher electrical conductivity of these layers compared with pure PEDOT:PSS layers is expected together with an increase in the extinction coefficient in the near-infrared range (Drude term). However, the reported extinction coefficient parallel to the surface plane is 15-20% larger (above 1000 nm) for the films of PEDOT:PSS prepared without sorbitol compared to those prepared with sorbitol. According to [24], the long wavelength absorbance could be a result of mid-gap states, and the change in the extinction coefficient is associated with the red shift of the absorbance maximum. Thus, sorbitol acts as a plasticizer which enables reorientation of polymer chains to a more random state and inter-chain interactions between the conducting polymers.

We report on the electrical, morphological and optical study of a series of spiral-bar coated single layers of PEDOT:PSS, influenced by the addition of different secondary dopants, 6 of which have been reported for the first time. The optical properties were studied over a wide spectral range using spectroscopic ellipsometry. The isotropic model was used to describe the measured data and the anisotropic model was introduced and its usefulness discussed. This paper deepens the results presented during poster session at the 26$^{th}$ International Conference on Amorphous and Nanocrystalline Semiconductors [25].

**2 Experimental** The layers were spiral-bar coated from custom made synthetized PEDOT:PSS 1:2.5 (COC Ltd.) water based dispersion (0.8 wt%). The secondary dopant in the amount of 5 wt% was added dropwise into the dispersion under mixing by a magnetic stirrer. The mixing was then continued for 6 hours. Prepared ink formulations were filtered by a PTFE syringe filter (0.45 μm) and then deposited using an automatic film applicator with a wire bar coater (TQC AB3120) using the 50 μm spiral bar. The dispersions with various secondary dopants (Methanamide, N-methyl methanamide, N,N-Dimethylacetamide, Dimethyl sulfoxide, Ethane-1,2-diol, propane-1,2-diol, Butane-1,2-diol, Tetrahydrothiophene 1,1-dioxide, N,N-Dimethylformamide, 2-Aminoethanol) were applied on float glass. The samples were dried in a hot air oven for 30 minutes at 120 °C.

The properties of the used secondary dopants [27, 28] are summarized in Table 1. All the used secondary dopants have quite high static dielectric constants and a boiling temperature higher than 120 °C, and they are soluble in water.

Two variable angle spectroscopic ellipsometers (VASE and IR-VASE J. A. Woollam Co.) were used for the optical characterization of the prepared samples. The first ellipsometer is equipped with an automatic rotating analyzer over the spectral range 190 nm – 1700 nm (UV-VIS-NIR), measuring 30 revolutions with photon

energy steps of 0.05 eV at three selected angles of incidence (AOI) (50°, 60° and 70°). The second ellipsometer is equipped with a rotating compensator for 1.7 μm – 30 μm (NIR-MIR), using AOI as above, measuring 20 scans, 15 spectra per revolution with wavenumber steps 16 $cm^{-1}$. Normal incidence optical transmittance was measured by the same instruments. WVASE32 software was used for modelling the measured data.

AFM measurements were performed using the Solver NEXT (NT-MDT Co., Russia) equipped with a NSG10 tip (NT-MDT Co., Russia) in semicontact (tapping) mode. Two measurements (spot size 3×3 μm) were performed on each sample and the average root mean square (RMS) of the surface roughness was determined according to the ISO 4287/1.

Electrical properties were measured via the 4 point method using a 6 ½ Digit Digital Multimeter Rigol DMM 3068 at room temperature 20 °C. The geometrical properties of conductive tracks between measuring electrodes were determined using optical microscopy (Leica DM750 M, ICC 50 HD Camera). The layer thicknesses were estimated using a mechanical profilometer (Dektak XT).

**Table 1** Physical properties of the spiral-bar coated samples with various secondary dopants / solvents; the data for the solvents are from [27, 28] and the specific electrical conductivity of samples was measured at the room temperature.

| sample | secondary dopant / solvent | static dielectric constant of solvent | boiling temperature of solvent (°C) | density of solvent ($g/cm^3$) | specific conductivity of sample (S/cm) |
|---|---|---|---|---|---|
| 1 | None | - | - | - | 0.3 |
| 2 | 2-aminoethanol ($C_2H_7NO$) | 38 | 170 | 1.012 | 2.4 |
| 3 | tetrahydrothiophene 1,1-dioxide ($C_4H_8O_2S$) | 44 | 285 | 1.261 | 19.8 |
| 4 | N,N-dimethylformamide ($C_3H_7NO$) | 37 | 153 | 0.944 | 25.6 |
| 5 | propane-1,2-diol ($C_3H_8O_2$) | 32 | 188 | 1.040 | 27.8 |
| 6 | butane-1,2-diol ($C_4H_{10}O_2$) | 20 | 195 | 1.002 | 29.5 |
| 7 | N,N-dimethylacetamide ($C_4H_9NO$) | 38 | 165 | 0.923 | 34.8 |
| 8 | ethane-1,2-diol ($C_2H_6O_2$) | 37 | 197 | 1.110 | 54.2 |
| 9 | methanamide ($CH_3NO$) | 111 | 210 | 1.130 | 69.0 |
| 10 | dimethyl sulfoxide ($C_2H_6OS$) | 47 | 189 | 1.100 | 70.3 |
| 11 | N-methyl methanamide ($C_2H_5NO$) | 186 | 183 | 1.003 | 78.3 |

## 3 Results and discussion

### 3.1 Electrical properties

The values of the evaluated specific electrical conductivity of the layers at room temperature are summarized in Table 1. As expected, because of the high static dielectric constant of the used secondary dopants, all the secondary dopants, except 2-aminoethanol, increased specific electrical conductivity by more than 2 orders of magnitude in comparison with the PEDOT:PSS sample without secondary dopant. The highest value of specific

electrical conductivity was achieved by using n-methyl methanamide as the secondary dopant. The measured values of specific electrical conductivity are comparable with the values found in the literature (25.6 S/cm for sample 4 <=> 30 S/cm using dimethyl formamide [11]; 70.3 S/cm for sample 10 <=> 80 S/cm using dimethyl sulfoxide [11]; 29.5 S/cm for sample 6 <=> 10 S/cm using diethylene glycol [14]). Reported values for conductivity using ethane-1,2-diol are significantly higher (around 700 S/cm) [7] <=> 54.2 S/cm for sample 8 as well as the conductivities enhanced using dimethylsulfoxide (966 S/cm) [8] <=> 70.3 S/cm for sample 10 what was given by using commercial grade of PEDOT:PSS dispersion PH 1000 from H. C. Starck. For our study we used custom made synthetized dispersion of PEDOT:PSS to have full control under the composition and additives content. Disadvantage of custom made dispersion is that the conductivity was not expected to be at level of the top commercial dispersion of PEDOT:PSS.

The data for the specific electrical conductivities were plotted against the static dielectric constant of the used secondary dopant / solvent (see Fig. 1). Dependence of specific electrical conductivity on static dielectric constant can be roughly divided into two parts (below 40 and over 40). It can be concluded that overall the influence of static dielectric constant on the conductivity is hardly to explain from our measurements. If we consider derives of methanamide (samples 4, 9 and 11 – labelled by red points in Fig.1) it can be concluded that higher dielectric constant lead to higher conductivity. The samples with the three highest specific electrical conductivities were prepared from secondary dopants / solvents having the highest static dielectric constants, but the relationship for whole set of solvents is not statistically very significant. Nevertheless, the role of the high static dielectric constant of given solvents in influencing the specific electrical conductivity of PEDOT:PSS layers is still evident. The high static dielectric constant of the used secondary dopants was reported to increase the screening effect [11], which might have an influence on the increased specific conductivity reported here.

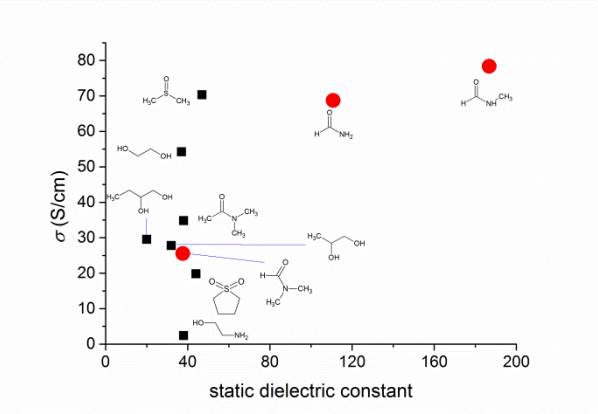


**Figure 1** Dependence of specific electrical conductivity on the static dielectric constant of used secondary dopant / solvent with its chemical formula depicted. Red circles denote derives of methanamide.

### 3.2 Morphological properties

A linear scratch was mechanically induced in the PEDOT:PSS layer to a depth where the layer/substrate interface was reached. The thickness of the layers was then estimated as the height of the obtained step via the profilometry measurement. From the AFM measurement, the root mean square surface roughness was calculated as a parameter describing the surface morphology of the samples. The thickness of the layers and the surface

roughness obtained using mechanical probes (profilometry + AFM) are summarized together with the results of the optical measurements in Figures 2 and 3 (histograms). The thicknesses obtained from isotropic model are close (difference maximally 25%) to the results measured using mechanical profilometry.

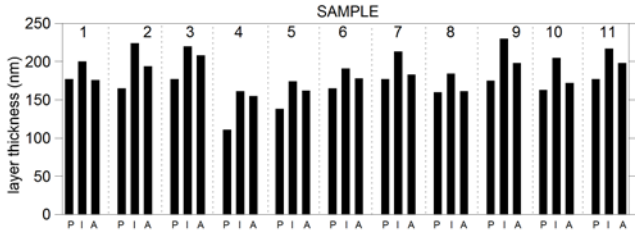


**Figure 2** Thickness of the layers determined via mechanical profilometry (P) and spectroscopic ellipsometry with isotropic model (I) and anisotropic model (A).

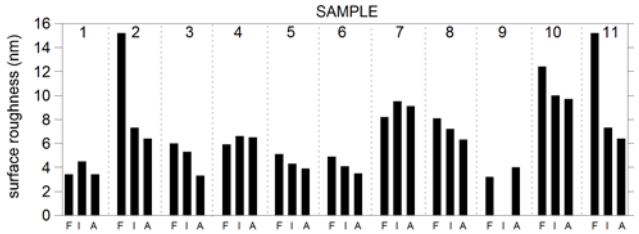


**Figure 3** Surface roughness of the layers determined by AFM (F) and spectroscopic ellipsometry with isotropic model (I) and anisotropic model (A).

From the results of the AFM surface roughness of the layers, it could be concluded that the layer roughness increases when the secondary dopant is involved in sample preparation; only one exception to this rule was found (sample 9). This conclusion is consistent with the results of previously reported papers [7-17].

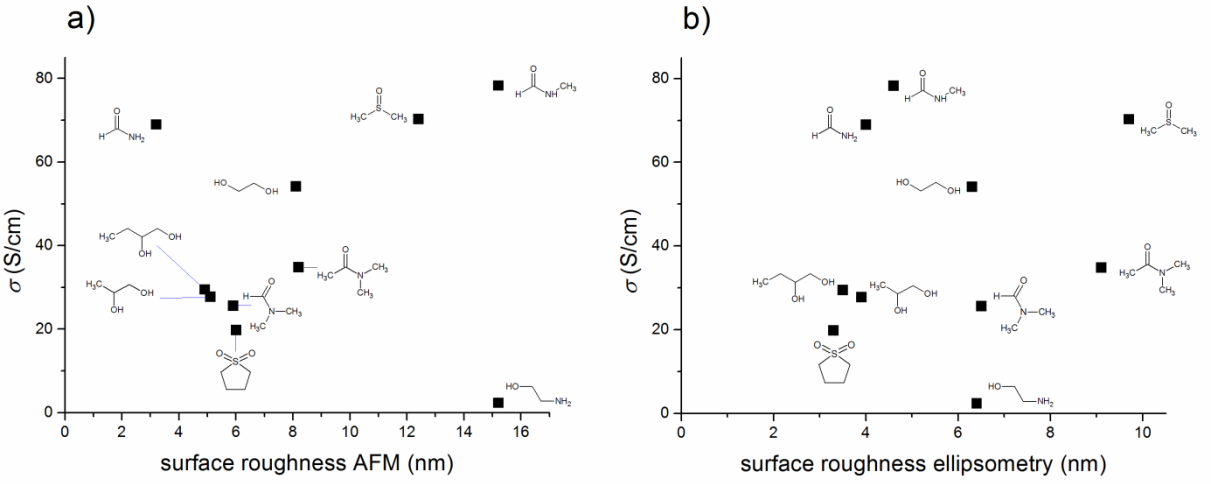


**Figure 4 a)** Dependence of specific electrical conductivity on the surface roughness obtained from AFM (left) and **b)** dependence of specific electrical conductivity on the surface roughness obtained from ellipsometry (right) with secondary dopant / solvent chemical formula depicted.

The data for the specific electrical conductivities were plotted against the surface roughness obtained from AFM (see Fig. 4a). Except two secondary dopants (2-aminoethanol = sample 2 and methanamide = sample 9) the obvious positive trend of specific electrical conductivity on the surface roughness can be identified. Conduction via surface states caused possibly by conformational reorganization might have an influence on the increased specific conductivity reported here as found also by Gasiorowski et al. [8]. Notice that when surface roughness obtained by ellipsometry is used the overall dependence of specific conductivity on the surface roughness is not clear (see Fig. 4b).

AFM image (Figure 5) of sample 8 shows PEDOT-rich particles, which are visible as darker areas. Although the electrical conductivity increases by three orders of magnitude, there is no significant difference in the appearance (reported e.g., in [7]) for any secondary dopant. This observation is consistent with previous work [29], where dimethyl sulfoxide, sorbitol, ethane-1,2-diol and N,N-dimethylformamide were used as secondary dopants. The study includes Raman spectroscopy analysis, which confirmed that the spectra of the doped PEDOT:PSS films obviously showed the same pattern as those of the undoped PEDOT:PSS. In the Raman spectra, no presence of secondary dopants was found after heat treatment of the films.

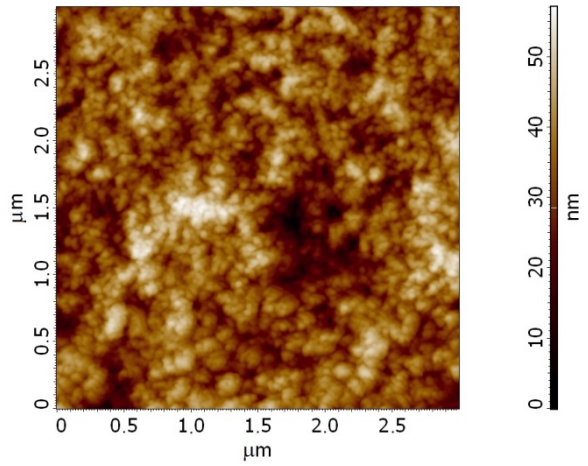


**Figure 5** Typical AFM image (sample 8).

**3.3 Optical properties** Spiral-bar coated layers were investigated using spectroscopic ellipsometry. The change of the polarization state is usually expressed by two parameters, amplitude ratio $\psi$ and phase shift Δ, that are defined using the Fresnel reflection coefficients for p- and s- polarized light:

$$\frac{r_p}{r_s} = tan(\psi) \cdot \exp(\mathrm{i}\Delta) \qquad (1)$$

Spectroscopic ellipsometry is an indirect optical characterization method, where the measured values $\psi^{exp}$ and $\Delta^{exp}$ are compared to the values calculated from the model. In the model structure, the optical constants of the layers and their thicknesses are assumed, and it is possible to calculate the corresponding values of $\psi^{mod}$ and $\Delta^{mod}$ belonging to the proposed model structure. Geometrical properties, such as thickness of the PEDOT:PSS layer and surface roughness, could also be determined as parameters of the model. In this way, the optical parameters of studied layers, such as complex refractive index (which includes refractive index as the real part and

extinction coefficient as the imaginary part) can be calculated. Computation of various parameters of the layers was performed via regression analysis, where the minimization procedure was based on the mean square error (MSE) values; MSE is given in the following expression:

$$MSE = \sqrt{\frac{1}{2N-M}\sum_{i=1}^{N}\left[\left(\frac{\psi_i^{mod}-\psi_i^{exp}}{\sigma_{\psi,i}^{exp}}\right)^2+\left(\frac{\Delta_i^{mod}-\Delta_i^{exp}}{\sigma_{\Delta,i}^{exp}}\right)^2\right]} \quad (2)$$

where $N$ is the number of measured pairs of ellipsometric parameters $\psi^{\exp}$ and $\Delta^{\exp}$ and $M$ represents the total number of fitted parameters. $\sigma_{\psi,i}^{exp}$ and $\sigma_{\Delta,i}^{exp}$ are then the estimated experimental error of $\psi^{\exp}$ and $\Delta^{\exp}$, respectively. Ellipsometric data measured for all three angles of incidence 50°, 60° and 70° were used in the fit simultaneously.

### 3.3.1 Isotropic model

In this approach, each of the films of secondary doped PEDOT:PSS was modeled as a homogenous optically isotropic layer. The sample model used for ellipsometry spectra analyses consists of: 1) a semi-infinite glass substrate (with optical constants obtained previously on a blank sample of uncoated float glass), 2) a homogenous, isotropic layer representing the secondary doped PEDOT:PSS, 3) surface roughness modeled by a Bruggeman type effective medium approximation of the 50% voids and 50% layers [31], and 4) air as the ambient medium.

The wide spectral range was split into two parts, where the measured data were processed differently. The UV-VIS-NIR part of the spectrum in the 0.7 – 6.5 eV range was fitted separately from the IR part of 0.035 eV – 0.7 eV.

The Lorentz multiple oscillator model was chosen as the model dielectric function, where the complex index of refraction is expressed as a function of photon energy, $h\nu$, as:

$$\tilde{N} = \left(\varepsilon_1(\infty) + \sum_{n=1}^{N}\frac{A_n}{E_n^2-(h\nu)^2-i\Gamma_n h\nu}\right)^{1/2} \quad (3)$$

Parameter $A_n$ corresponds to the intensity, $\Gamma_n$ denotes the wideness, $E_n$ denotes the center energy of the $n$-th oscillator, and $\varepsilon_1(\infty)$ denotes the dielectric function at infinite energy.

The isotropic model fits to the measured data quite well, and the goodness-of-fit test defined by MSE was less than 10. The quality of fitting of the experimental data for sample 4 is shown in Figure 6, where the goodness-of-fit test MSE is equal to 6.4.

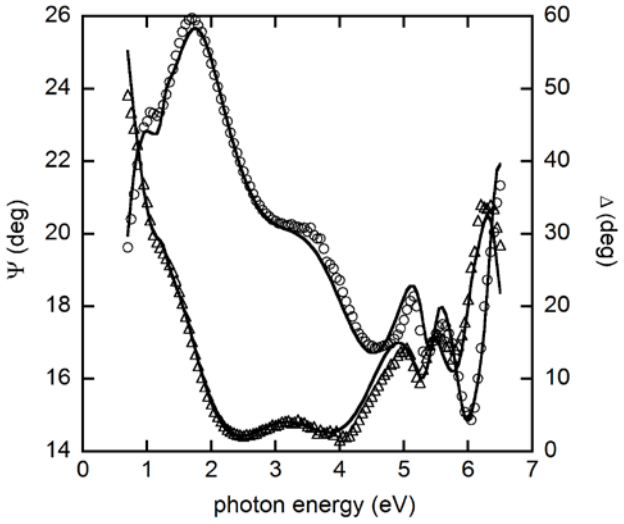


**Figure 6** Measured values of $\psi$ (circles) and Δ (triangles) for UV-VIS part of spectra of sample 4 together with the best fit (solid line) using the isotropic model for the angle of incidence 70°.

From the regression analysis, the imaginary part of the complex refractive index (extinction coefficient) was calculated. Overall, the extinction coefficient exhibits a similar spectral behavior for all the studied samples. UV part of the spectra was fitted by two Lorentz oscillators with central energies within the interval $E_{n1} \in (5.39,\ 5.66)$ eV and $E_{n2} \in (6.33, 6.5)$ eV for all the studied samples. These transitions are close to those previously reported in the literature, they were attributed to the p-p* transitions of the benzene rings of PSS [23-25]. The NIR part of spectra contains similar values of the extinction coefficient for all samples, showing that the response in the NIR spectrum was not influenced by the used secondary dopants. This part of the spectrum has been frequently described using the Drude term (free carrier contribution). It will be shown later that when the MIR spectral range is considered, the Drude term should be replaced by the sum of Lorentz terms.

There are no significant differences between either the refractive index *n* or the extinction coefficient *k* among all the samples with different electric conductivities, which is in contrast with the results reported by Gasiorowski et al. [8]. (See Figure 7 for samples 1 and 11, which are the samples with the lowest and the highest value of the electrical conductivity).

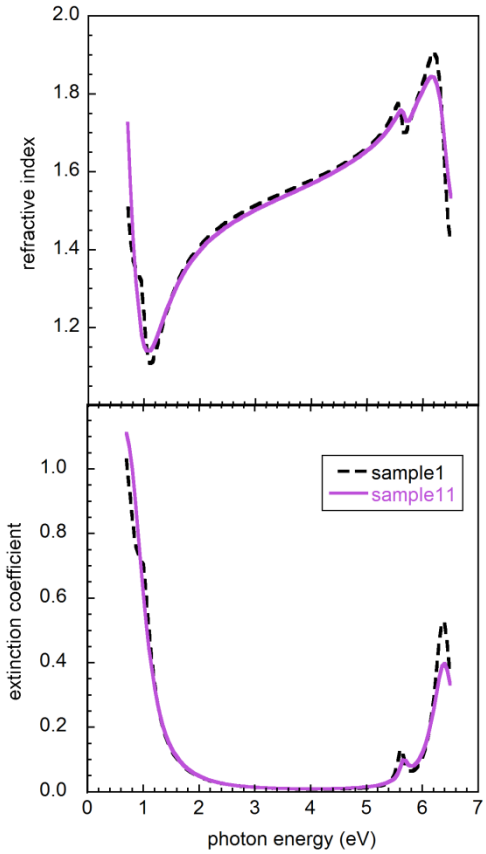


**Figure 7** Comparison of the refractive index (upper part) and the extinction coefficient (lower part) as a function of photon energy for UV-VIS part of spectra obtained using the isotropic model for samples 1 (black dashed line) and 11 (purple solid line) having the lowest and the highest specific electrical conductivity, see Table 1.

The second part of the spectral range, i.e., the MIR part (0.035 eV – 0.7 eV), was fitted using the same 4 layer model. The thickness was introduced from previous regression analysis of the UV-VIS part of spectra and with the optical constant of the secondary doped PEDOT:PSS layer modeled again by a sum of Lorentz oscillators. Similar to the analysis of the UV-VIS part of the spectra, the isotropic model fits the data quite well, with the MSE being less than 3. Thus, it could be claimed that the given model corresponds very well to these data. The quality of the fitting for sample 9 is displayed in Figure 8, where MSE = 1.1.

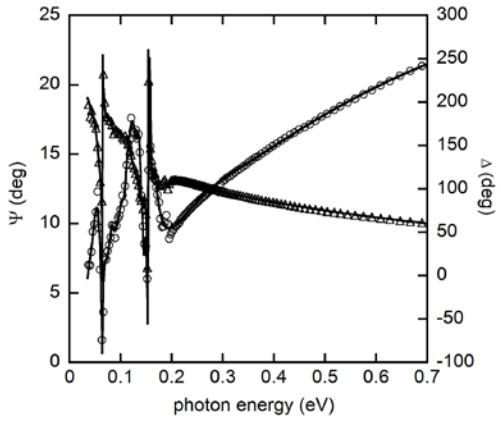

**Figure 8** Measured values of $\psi$ (circles) and $\Delta$ (triangles) for MIR part of spectra of sample 9 together with the best fit (solid line) using the isotropic model for the angle of incidence 70°.

Figure 9 shows comparison of the refractive index and the extinction coefficient for samples 1 and 11, which are the samples with the lowest and the highest values of the electrical conductivity, respectively. The similarity of both is evident.

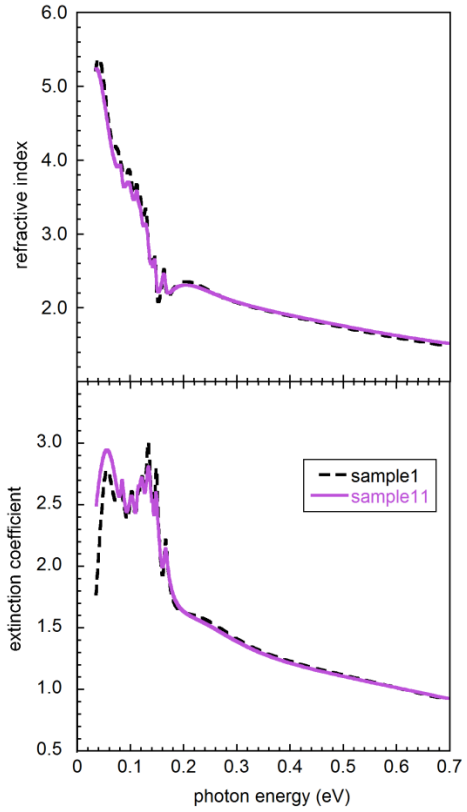


**Figure 9** Comparison of the refractive index (upper part) and the extinction coefficient (lower part) as a function of photon energy for MIR part of spectra obtained from the isotropic model for samples 1 (black dashed line) and 11 (purple solid line) having the lowest and the highest value of specific electrical conductivity, see Table 1.

Generally, two different features can be observed in the spectral dependence of the extinction coefficient in the MIR. A total number of 11 Lorentz oscillators used for its description consists of 3 broad Lorentz oscillators and 8 narrow ones. When focusing on the 3 broad oscillators, we assigned them to so called “mid-gap states”. We supposed the existence of many electronic states (bands) within the bandgap, analogous to the typical behavior of amorphous materials because of the complicated structure of the polymer layer. Electronic transitions appear within the bandgap or between valence/conduction bands, whereas the gap states are present in the MIR part of spectra. Applying the molecular orbital picture, the charge transfer between different molecules or within molecule could be attributed to these MIR absorptions, although the so-called “mid-gap states” have not been modeled previously. Notably, using the Drude model to describe the free carrier absorption is likely not valid here. We supposed that the MIR optical frequencies excite only a fraction of the electronic transitions. Whether any of these transitions could be assigned to hoping transport measured in DC conductivity is not clear while the samples with very similar extinction coefficients present up to 2-3 orders-of-magnitude different electrical conductivities.

The 8 narrow oscillators present at wavenumbers smaller than 2000 $cm^{-1}$ (0.25 eV) were assigned to narrow resonance vibrational lines, which are superposed on previously described broad Lorentz oscillators. Because a low resolution used in our measurement (16 $cm^{-1}$), fewer vibrations modeled by narrow Lorentz oscillators were found in the range 500 to 2200 $cm^{-1}$ than those reported in [32-33].

The consecutive step in the creation of the isotropic model merges both measurements together, which enabled the use of the model with the sum of Lorentz oscillators for the whole spectrum. This process was performed for all samples with MSE of approximately 6 or less. For practical use of PEDOT:PSS + secondary dopant layers, it is important that they provide high transparency and good electrical conductivity. Comparison of the transmittance of the layers measured on a bare glass substrate and sample 11 (having the highest electrical conductivity) is depicted at Figure 10, where the short wavelength as well as the long wavelength absorption edges of the glass substrate are clearly visible. This figure demonstrates reasonable optical transparency of the studied samples, especially in the visible part of the spectrum.

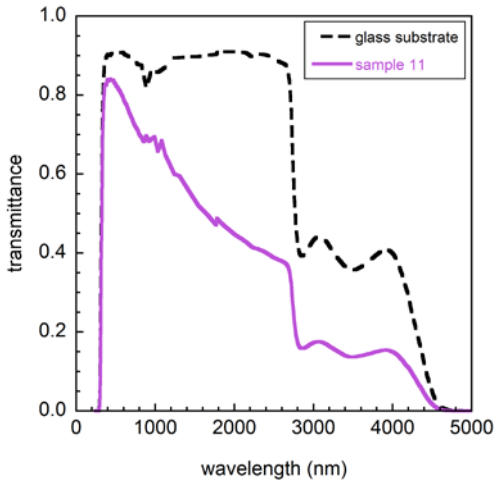


**Figure 10** Comparison between the transmittance measured through the bare float glass substrate (black dashed line) and the transmittance of glass + sample11 (purple solid line) with the highest value of specific electric conductivity.

Geometrical parameters (thickness of layers and surface roughness) obtained using the isotropic model are summarized in Figures 2 and 3.

In spite of increased specific electrical conductivity by 2-3 orders of magnitude when the secondary dopant is used, there is no such large difference in the optical constants. Furthermore, the optical constants of doped and undoped PEDOT:PSS layers are very similar, as suggested in [29]. Thus, we may conclude that increasing the DC electric conductivity by secondary dopants is not necessarily connected with the change of the optical properties of samples. It is very likely that incorporation of secondary dopants introduces morphological changes (conformational changes [7, 9]) of the PEDOT:PSS spatial arrangement in the layers, preferably leading to the conducting PEDOT arrangement. The differences in spatial arrangement were not found in the AFM analysis; however, they could likely cause an impact in the molecular fingerprint spectral region.

The isotropic model was successfully used by [6] in the case of PEDOT:PSS layers prepared by the electrospray method onto indium-tin-oxide (ITO) substrates. It was concluded that the type of growth (isotropic

vs. anisotropic) originates from a preferential orientation of the polymer chains obtained in the preparation process, the applied sort of substrate, and its morphology, and the growth depends on the film thickness.

**3.3.2 Anisotropic model**

Because of the lack of direct access to the sample morphology, it is not clear yet if the spiral-bar coated samples exhibit optical anisotropy. As mentioned before, according to previous research results [24], the anisotropic model with different in-plane and out-of-plane refractive indexes and extinction coefficients were considered for the spin coated samples. The *xz* plane is the plane of incidence. The optical response of layer is described by an ordinary complex index of refraction parallel to the surface plane (*xy* plane, $\widetilde{N}_{\text{in-plane}} = \widetilde{N_x} = \widetilde{N_y}$) and an extraordinary index of refraction perpendicular to the surface plane ($\widetilde{N}_{out-of-plane} = \widetilde{N_z}$).

Using the previously obtained optical constants described by the sum of Lorentz oscillators independently for in-plane and out-of-plane optical constants, the model has very large number of possible correlated parameters. Attempting to fit the many oscillators in this range independently, result in the values without any physical meaning, especially for describing the out-of-plane optical constants. This result, in our opinion, is a strong disadvantage of using the anisotropic model.

To address this problem, the anisotropic UV-VIS optical constant were adopted from the study of Pettersson et al. [24], with the aim to expand the optical constants to the MIR. We attempted to describe the in-plane hopping transport via the Lorentz term, giving the optical response of a polaron with central energy in the IR part of spectra. Because three Lorentz oscillators were not sufficient to describe the in-plane behavior, one more Lorentz oscillator was added in the IR region. In the out-of-plane spectra, one Lorentz term with three parameters (center energy – same as last oscillator from in-plane, wideness and intensity) was used.

The geometric parameters (thickness of layers and surface roughness) obtained using anisotropic model are summarized in Figures 2 and 3. When comparing geometrical parameters obtained via spectroscopic ellipsometry with those obtained using mechanical methods (profilometry and AFM), the isotropic model provides thicker layers, but the anisotropic model gives thicknesses closer to mechanical profilometry. Due to closeness of the thickness results for all methods, we consider the accuracy of obtaining the thickness with spectroscopic ellipsometry sufficient in the cases of both of the used models.

In both cases (isotropic and anisotropic model), the surface roughnesses are in very good agreement with the AFM measurements, with the only exception (sample 9 isotropic model) being where the fitted value of surface roughness decreases to zero.

The optical constants for PEDOT:PSS prepared without solvent (sample 1) obtained using the anisotropic model are presented in Figure 11.

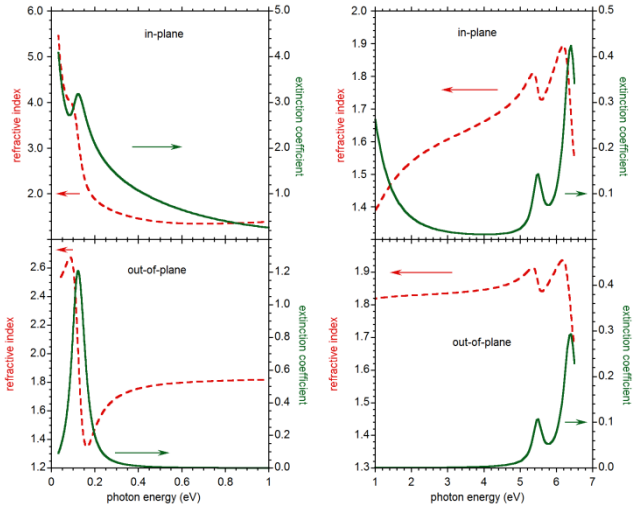


**Figure 11** Refractive index (red dashed line) and extinction coefficient (green solid line) of sample 1 as a function of photon energy obtained from the anisotropic model for in-plane (upper part) and out-of-plane (lower part). Notice different scale for in-plane and out-of-plane optical constants.

The applied model does not provide a good fit to the IR fingerprint vibrations that were ignored here for the simplicity. Nevertheless, using this approach, it is possible to describe the optical constants of PEDOT:PSS + secondary dopant layers using the anisotropic model with MSE below 9, which is generally worse than the MSE obtained for the isotropic model. The validity of this model is therefore questionable.

General conclusions can be consistently found by comparing the results obtained by the isotropic and anisotropic models.

Although many previous works recommended application of the anisotropic model for PEDOT:PSS layers, we successfully evaluated the spectroscopic data using the isotropic model. This result can be due to the different methods of samples preparation (spin coating vs. spiral-bar coating). Moreover, using of the isotropic model was reported in earlier literature [6]. Thus, in further research, we prefer to use the isotropic model instead of the anisotropic model.

## 4 Conclusions

The electrical, morphological and optical properties of spiral-bar coated layers were studied. The layers were prepared from PEDOT:PSS dispersions modified with 10 different secondary dopants / solvents, where 6 of these solvents were not previously reported in the literature.

The selected solvents caused an increase of the specific electric conductivity in the range of 2.4 to 78.3 S/cm, which is more than two orders-of-magnitude higher than the value of 0.3 S/cm measured for layers prepared from the pure PEDOT:PSS dispersion. The highest increase in specific electrical conductivity (78.3 S/cm) was measured for the sample prepared using the secondary dopant / solvent of N-methyl methanamide, which is much more efficient than generally used dimethyl sulfoxide.

The aim of the work was also focused on finding a non-destructive and contactless technique for the evaluation of thickness of secondary doped PEDOT:PSS layers. For this purpose, the UV/VIS ellipsometry technique was used in combination with AFM and mechanical profilometry techniques. The estimated film thickness (~ 200 nm) and surface roughness determined via UV and VIS ellipsometry measurements were found

to be consistent with the above-mentioned standard characterization tools (mechanical profilometry, AFM). Ellipsometry, unlike profilometry, has the advantage in absence of risk of local film removal (scratch). Hence, ellipsometry is concluded to be a reliable and non-destructive tool for layer thickness determination.

From the goodness of fit test of regression analysis, the optical constants (refractive index and extinction coefficient) of PEDOT:PSS layers, prepared with 10 different secondary dopants in broad spectral range from UV to MIR (0.19 - 30 μm), could be described/fitted by the isotropic model. However, no substantial differences in the optical constants were observed, despite such differences being expected from the significant change of specific electrical conductivity (3 orders of magnitude). It was found that the near-infrared part of the spectrum that is frequently fitted by the Drude term in the literature could be better described by the model of the multiple Lorentz oscillators describing (a) the narrow molecular fingerprint vibrations superposed on (b) broad electronic transitions inside/among mid-gap states. The connection of these Lorentz oscillators to hoping transport/polaron is likely improbable due to the similarity of the optical constants obtained for all samples. Using the anisotropic model resulted in the same conclusion, where again, no significant differences were found among the optical constants of the studied samples. From the regression analysis results and from the point of view of simplicity of the fitting calculation, the isotropic model was preferred. The isotropic model was more suitable for the fitting of the given data sets, probably due to the use of the spiral-bar coating method, which likely influenced the arrangement of the polymer chains during deposition and formation of the wet layer.

In this paper, we demonstrated that spectroscopic ellipsometry is a non-destructive characterization technique that provides important feedback for the development of PEDOT:PSS layers from aqueous dispersions with the presence of different secondary dopants / solvents produced using the spiral-bar coating technique. Spectroscopic ellipsometry can be beneficial for the characterization of PEDOT:PSS layers prepared on flexible substrates and therefore appears to be a valuable tool for the characterization of functional layers used in printed electronics.

**Acknowledgements** Financial support from the Technology Agency of the Czech Republic (project No. TE01020022) and projects LM2015082 and CZ.1.05/4.1.00/11.0251 “Center of Materials and Nanotechnologies” co-financed by the European Fund of the Regional Development and the state budget of the Czech Republic are gratefully acknowledged. Support of the COST Action FP1405 ActInPack is gratefully acknowledged.

Authors would like to acknowledge doc. V. Zima from Joint Laboratory of Solid State Chemistry of the Institute of Macromolecular Chemistry of AS CR and University of Pardubice and Dr. V. Pejchal from Institute of Organic Chemistry and Technology of University of Pardubice for valuable comments, suggestions and discussion.

## References

[1] A. C. Grimsdale, K. L. Chan, R. E. Martin, P. G. Jokisz, A. B. Holmes, Chem. Rev. 109 (2009) 897–1091.

[2] R. Po, C. Carbonera, A. Bernardi, F. Tinti, N. Camaioni, Solar Energy Materials and Solar Cells 100 (2012) 97–114.

[3] S. Nambiar, J.T.W. Yeow, Biosensors and Bioelectronics 26 (2011) 1825-1832.

[4] K. Sun, S. Zhang, P. Li, Y. Xia, X. Zhang, D. Du, F.H. Isikgor, J. Ouyang, Journal of Materials Science: Materials in Electronics 26 (2015) 4438-4462.

[5] D.S. Germack, C.K. Chan, R.J. Kline, D.A. Fischer, D.J. Gundlach, M. F. Toney, L.J. Richter, D.M. DeLongchamp, Macromolecules 43 (2010) 3828-3836.

[6] T. Ino, T. Hiate, T. Fukuda, K. Ueno, H. Shirai, J. Non-Cryst. Solids 358 (2012) 2520-2524.

[7] Y.H. Kim, Ch. Sachse, M.L. Machala, Ch. May, L. Müller-Meskamp, K. Leo, Adv. Funct. Mater. 21 (2011) 1076-1081.

[8] J. Gasiorowski, R. Menon, K. Hingerl, M. Dachev, N.S. Sariciftci, Thin Solid Films 536 (2013) 211-215.

[9] J. Ouyang, Q. Xu, Ch.-W. Chu, Y. Yang, G. Li, J. Shinar, Polymer 45 (2004) 8443-8450.

[10] J. Ouyang, Ch.-W. Chu, F.-Ch. Chen, Q. Xu, Y. Yang, Adv. Funct. Mater. 15 (2005) 203-208.

[11] J.Y. Kim, J.H. Jung, D.E. Lee, J. Joo, Synthetic Met. 126 (2002) 311-316.

[12] S.K.M. Jönsson, J. Birgerson, X. Crispin, G. Greczynski, W. Osikowicz, A.W.D. van der Gon, W.R. Salaneck, M. Fahlman, Synthetic Met. 139 (2003) 1-10.

[13] T.Y. Kim, J.E. Kim, K.S. Suh, Polym. Int. 55 (2006) 80-86.

[14] X. Crispin, F.L.E. Jakobsson, A. Crispin, P.C.M. Grim, P. Andersson, A. Volodin, C. van Haesendonck, M. Van der Auweraer, W.R. Salaneck, M. Berggren, Chem. Mater. 18 (2006) 4354-4360.

[15] F. Zhang, M. Johansson, M.R. Andersson, J.C. Hummelen, O. Inganäs, Adv. Mater. 14 (2002) 662-665.

[16] S.A. Mauger, A.J. Moulé, Organic Electronics 12 (2011) 1948-1956.

[17] C.S. Lee, J.Y. Kim, D.E. Lee, Y.K. Koo, J. Joo, S. Han, Y.W. Beag, S.K. Koh, Synthetics Met. 135-136 (2003) 13-14.

[18] A.M. Nardes, M. Kemerink, R.A.J. Janssen, Phys. Rev. B 76 (2007) 085208-1-7.

[19] A.M. Nardes, M. Kemerink, R.A.J. Janssen, J.A.M. Bastiaansen, N.M.M. Kiggen, B.M.W. Langeveld, A.J.J.M. van Breemen, M.M. de Kok, Adv. Mater. 19 (2007) 1196-1200.

[20] J. Huang, P.F. Miller, J.S. Wilson, A.J. de Mello, J.C. de Mello, D.D.C. Bradley, Adv. Funct. Mater. 15 (2005) 290-296.

[21] S. Timpanaro, M. Kemerink, F. Touwslarger, M.M.D. Kok, S. Schrader, Chem. Phys. Lett. 394 (2004) 339-343.

[22] S. Logothetidis, A. Laskarakis, Thin Solid Films 518 (2009) 1245-1249.

[23] L.A.A. Pettersson, F. Carlsson, O. Inganäs, H. Arwin, Thin Solid Films 313-314 (1998) 356-361.

[24] L.A.A. Pettersson, S. Ghosh, O. Inganäs, Organic Electronics 3 (2002) 143-148.

[25] T. Syrovy, P. Janicek, J. Mistrik, K. Palka, P. Hawlova, L. Kubac, M. Klanjšek Gunde, Optical, electrical and morphological study of PEDOT:PSS single layers spin coated with various secondary doping solvents optimized for printed electronics, poster presented at: 26th International Conference on Amorphous and Nanocrystalline Semiconductors, 13-18 September 2015, Aachen, Germany.

[26] M. Losurdo, K. Hingerl (eds.), Elipsometry at the Nanoscale (Springer-Verlag, Berlin Heidelberg, 2013).

[27] I.M. Smallwood, Handbook of organic solvent properties (Elsevier, Oxford, 1996).

[28] Knovel Critical Tables (2nd Edition), (Knovel, 2008). Online version available at: http://app.knovel.com/hotlink/toc/id:kpKCTE000X/knovel-critical-tables/knovel-critical-tables.

[29] J. Nevrela, M. Micjan, M. Novota, S. Kovacova, M. Pavuk, P. Juhasz, J. Kovac Jr., J. Jakabovic, M. Weis, J. Polym. Sci. Pol. Phys. 53 (2015) 1139-1146.

[30] H.G. Tompkins, E.A. Irene, Handbook of Ellipsometry (Springer-Verlag, Heidelberg, 2005).

[31] D.A.G. Bruggeman, Ann. Phys. (Leipzig) 24 (1935) 636-664.

[32] M. Schubert, C. Bundesmann, G. Jakopic, H. Maresch, H. Arwin, N.-C. Persson, F. Zhang, O. Inganäs, Thin Solid Films 455-456 (2004) 295-300.

[33] M. Schubert, C. Bundesmann, H. v. Wenckstern, G. Jakopic, A. Haase, N.-K. Persson, F. Zhang, H. Arwin, O. Inganäs, Appl. Phys. Lett. 84 (2004) 1311-1313.